



Optical Magnetism in Surface Plasmon Resonance–Based Sensors for Enhanced Performance

Md. Mahbub Hossain¹ · Muhammad Anisuzzaman Talukder¹

Received: 21 February 2020 / Accepted: 26 October 2020
© Springer Science+Business Media, LLC, part of Springer Nature 2020

Abstract

Surface plasmon resonance (SPR)–based structures are finding important applications in sensing biological as well as inorganic samples. In SPR techniques, an angle-resolved reflection (R) profile of the incident light from a metal-dielectric interface is measured and the resonance characteristics are extracted for the identification of the target sample. However, the performance, and hence the applicability of these structures, suffers when the weight and concentration of the target samples are small. Here, we show that SPR-based sensors can create strong magnetism at optical frequency, which can be used for the detection of target samples instead of using the conventional R profiles, as the magnetic resonance varies depending on the refractive index of the target sample. Using scattering parameters retrieval method, we computationally find out the effective permeability (μ_{eff}) of a SPR sensor with a structure based on Kretschmann configuration, and use it to calculate the performance of the sensor. A comparison with the conventional technique that uses R profile to detect a target sample shows a significant increase in the sensor performance when μ_{eff} is used instead.

Keywords Optical magnetism · Surface plasmon resonance · Effective permeability · Scattering parameters

Introduction

In the last few years, nano-structures have been studied and developed for magnetic responses. In particular, enhancing magnetic responses of dielectric layered structures at visible wavelength range has drawn significant interest due to their promising applications in sensors and exploitation of the non-linear properties that they offer [1–3]. Naturally, the magnetic response of most dielectric materials is weak, especially in the optical frequency range [4]. Additionally, planar multi-layer dielectric structures also show a relatively non-magnetic behavior with a very small magnetic permeability (μ_{eff}) [5–7]. However, multi-layer dielectric structures are promising in enhancing μ_{eff} due to their immense capability of being engineered in geometry and layer thicknesses. Recently, significant magnetic responses have been achieved in metal-insulator-metal structures by exciting Fano resonances and in planar

dielectric-metal multi-layer structures, where dielectric layers are isolated by air and silver layers [8]. Although the significant magnetism obtained from these structures makes these structures promising for sensing applications, they are not favorable for sensing due to creating multiple Fano resonances through anti-phase dipole oscillations, and hence, forming destructive interference, and also due to the complexity in the structures. A U-shaped split ring resonator designed by metal-dielectric multi-layer structure has also been proposed for enhanced magnetization, which has potential for sensing applications as well [9]. However, applications of these structures could be limited due to the complexity in the fabrication of the practical devices.

The property of evanescent electromagnetic fields of surface plasmon polaritons (SPPs) in a planar metal-dielectric structure is used in many sensing techniques. However, the applications of surface plasmon resonance (SPR)–based sensors become limited while detecting small molecular weight (< 8 kDa) and low concentration (< 1 pM) analytes, which is often the case for several critical biological samples [10]. Recently, several SPR sensors have been proposed that show hyper sensitivity (S) so that molecules with less than 8 kDa weight and 1 pM concentration can be detected [11–13]. Although S is increased in the hyper sensitive structures by making

✉ Muhammad Anisuzzaman Talukder
anis@eee.buet.ac.bd

¹ Department of Electrical and Electronic Engineering,
Bangladesh University of Engineering and Technology,
Dhaka, 1205, Bangladesh

the structures complex, e.g., by adding additional layers, the angle-resolved reflectivity (R) profile is significantly broadened. The increase of full-width at half-maximum (FWHM) of the R profile causes the figure-of-merit (FoM) of the structure to decrease, which is the most critical performance parameter for such SPR sensors [14]. Additionally, several hybrid SPR sensors [15, 16] and SPR sensors with additional complexity by including black phosphorus, metamaterials, silicon, and MoS₂ nanostructures have shown to enhance S and FoM [17–20]. Recently, the addition of graphene and BaTiO₃ layers in SPR sensor has shown that the resonance angle can be shifted significantly with a small change of refractive index of the target sample [21]. Caballero et al. proposed magneto-optical SPR sensor, where the detection is based on the calculations of the transverse magneto-optical Kerr effect [22]. However, these hybrid SPR sensors often include complex arrangements of nano-structures, and need complicated and expensive manufacturing techniques.

SPR sensors based on Kretschmann configuration are the best choice for many sensing applications because of their simple structural arrangements. In SPR sensors, the presence of a biomolecule or any other target molecule in the sensing layer changes the SPR electromagnetic fields. The plasmonic characteristics and applications of SPR sensors have been explored well. However, SPR sensors usually show weak magnetic property and their magnetic properties have never been used for sensing. Optical magnetism in the optical frequency range using insulator-metal-insulator (IMI) Kretschmann plasmonic structure has not been explored till now. Similar to SPR resonances, strong magnetic resonances, also known as magnetic plasmons, can be excited in a multi-layer structure [23]. The concept is based on designing IMI planar multi-layer structures that support localized surface plasmons (LSPs), which act as magnetic dipoles and thus create strong optical magnetism. Thus, the enhanced localization of light by LSPs increases the magnetic response of the IMI planar multi-layer structure [24].

In this work, we show that an SPR sensor based on Kretschmann configuration can create strong magnetic response in optical frequency range in the presence of a target sample, and thus, magnetic property of these structures can be used to increase the performance in sensing the target sample. Using finite difference time domain (FDTD) simulations and scattering parameters (S -parameters) retrieval method, we calculate angle-resolved μ_{eff} and R profiles of a SPR sensor that has a structure based on Kretschmann configuration. We show that the FoM of the sensor based on the magnetic resonance increases significantly compared to that of a conventional purely SPR-based sensor. Exploitation of the magnetic property of the simple Kretschmann configuration has the potential of

obviating the need of a more complex sensor structure while achieving high sensor performance.

The rest of the paper is organized as follows: In Section “[Theoretical Modeling](#)”, we describe the theoretical models that we used to calculate μ_{eff} and R using S -parameters retrieval method. In Section “[Sensor Structure and Simulation Setup](#)”, we discuss the Kretschmann configuration-based SPR sensor structure investigated in this work and the FDTD simulation approach. In Section 1, we discuss a feasible experimental setup for the proposed sensing technique. In Section “[Results and Discussion](#)”, we present and discuss the calculated magnetic response of the sensor, and also the S and the FoM of the sensor calculated from μ_{eff} and R profiles. In Section “[Conclusion](#)”, we draw conclusions on the findings.

Theoretical Modeling

The electromagnetic response of a structure with a complex μ_{eff} can be determined through systematic Drude-Lorentz representation [25] or S -parameters retrieval technique [26–29]. Often, the Drude-Lorentz analytical model is not precise, especially, if the structure is a planar multi-layer. Alternatively, the S -parameters retrieval technique depends on the reflection (S_{11}) and transmission (S_{21}) coefficients assuming a real index of the medium, and gives more precise results for μ_{eff} [26]. The coefficients S_{11} and S_{21} are computed from amplitude and phase of the peak fields as recorded on the detection planes. The S -parameters retrieval technique assumes that the detection planes are far away from the metal-sample layer interface so that the fields can be assumed to be propagating like a plane wave. Practically, the distance of the detection plane for the reflected waves from the metal-sample layer interface and the distance of the detection plane for the transmitted waves from the metal-sample layer interface must be much greater than the wavelength of the incident light. It is also essential to recompense for the phase that gathers as the fields spread through the background medium from the source to the multi-layer structure, and from the multi-layer structure to the detection planes. Thus, using the S -parameters retrieval technique, μ_{eff} can be calculated by the following equations [26]

$$S_{11} = \frac{i}{2} \left(\frac{1}{z} - z \right) \sin(n_{\text{eff}} k_0 z), \quad (1a)$$

$$S_{21} = \frac{1}{\cos(n_{\text{eff}} k_0 d) - \frac{i}{2} \left(z + \frac{1}{z} \right) \sin(n_{\text{eff}} k_0 d)}, \quad (1b)$$

$$n_{\text{eff}} = \frac{1}{k_0 d} \cos^{-1} \left[\frac{1}{2S_{21}} (1 - S_{11}^2 + S_{21}^2) \right], \quad (1c)$$

$$z = \pm \sqrt{\frac{(1 + S_{11})^2 - S_{21}^2}{(1 - S_{11})^2 - S_{21}^2}}, \tag{1d}$$

$$\epsilon_{\text{eff}} = \frac{n_{\text{eff}}}{z}, \tag{1e}$$

$$\mu_{\text{eff}} = n_{\text{eff}}z, \tag{1f}$$

where n_{eff} is the effective refractive index, ϵ_{eff} is the effective permittivity, z is the normalized impedance, d is the total thickness of the multi-layer structure, i.e., the sum of the thicknesses of the different layers, and $k_0 = 2\pi/\lambda$, where λ is the wavelength of the incident light. To determine the effective constitutive parameters precisely, we follow the condition $k_0d < 1$ as $d < \lambda$ [26]. The reflectivity R can be determined as

$$R = |r_p|^2, \tag{2}$$

where r_p is the reflection coefficient for p -polarized incident light calculated using S -parameters retrieval method.

In this work, we will show that μ_{eff} of the multi-layer structure at resonance can be used to detect a target sample instead of using R at resonance. Practically, μ_{eff} can be precisely measured by several off-the-shelf devices, such as by a Ferromaster, which is a handy instrument capable of measuring μ_{eff} precisely [30]. The magnetic resonance angle is identified as the angle at which μ_{eff} reaches maximum while varying the incidence angle of light. The S of the multi-layer structure can be calculated as a change in the incidence angle for per unit change in the refractive index (n_s) of the sample, where the change in the angle can be due to the resonance for μ_{eff} as proposed in this work or for R as in conventional SPR excitation. The FoM depends inversely on the broadening of the FWHM of the response

profiles. Thus, we can write the S and FoM considering μ_{eff} or R at resonance as

$$S_{\mu,R} = \frac{\Delta\theta_{\mu,R}}{\Delta n_s}, \tag{3}$$

$$\text{FoM}_{\mu,R} = \frac{S_{\mu,R}}{\text{FWHM}}, \tag{4}$$

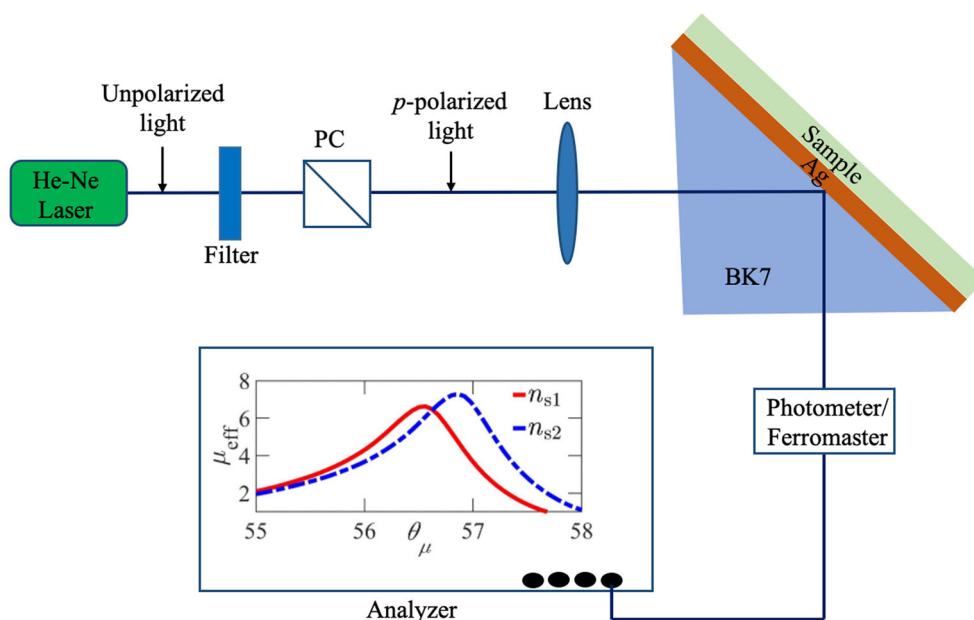
where $\Delta\theta$ and Δn_s are the changes in the incidence angles and the refractive index of the target sample, respectively. The subscripts μ and R represent whether the change in the angle is due to magnetic resonance or SPR, respectively.

Sensor Structure and Simulation Setup

The SPR Kretschmann configuration sensor structure consists of three different layers, as schematically shown in Fig. 1. The first layer is a semi-infinite prism of glass material, e.g., BK7. The exciting light is incident on the metal layer through the semi-infinite prism, and also the reflected light is collected from the semi-infinite prism. The second layer is metal, e.g., silver (Ag), which has a thickness of 45 nm. The third layer is the sample layer, which has a thickness of 50 nm. We assume that the incident light has a wavelength of 633 nm, which is often used in SPR-based systems for excitation [31, 32]. The refractive indices of different sensor layers are frequency dependent. The refractive index of BK7 has been calculated using the approach described in Ref. [33] and found to be 1.515 at 633 nm. The refractive index of Ag has been calculated using the Drude-Lorentz model [34].

We take the refractive index of the sample layer as a parameter and vary from 1.3 to 1.9. There are several

Fig. 1 Schematic illustration of a feasible experimental setup for the proposed technique



organic samples with a refractive index in this range. While different proteins and biomarkers have refractive indices in the range of 1.3–1.45 such as human fibrinogen (Fb) protein molecules and thyroglobulin (Tg) have refractive indices 1.39 and 1.45, respectively [35, 36], several other important organic samples such as benzene (C_6H_6), potassium hydrogen phthalate ($C_8H_5KO_4$), air-dried herring DNA (H-DNA), cyclotetramethylenete-tranitramine (HMX), and tetrahydrofuran (THF) clathrate have refractive indices in the range of 1.5–1.9 [37, 38].

To find out the dynamics of the incident light with the sensor in the presence of the target sample, we carry out two-dimensional full-field FDTD simulations. The simulation domain is $7\ \mu\text{m}$ in the direction of the layer interfaces, i.e., in the y -direction, and $8.5\ \mu\text{m}$ in the direction perpendicular to the interfaces, i.e., in the x -direction. We use a non-uniform meshing scheme for the computational domain to optimize the computational efficiency and accuracy of FDTD solutions. We use the perfectly matched layer boundary condition at the edges of the simulation domain in the direction perpendicular to the layer interfaces. We use Bloch boundary condition in the direction of the interfaces. The incident light has a transverse magnetic polarization and the incidence angle varies from 54° to 64° . The detection planes for the reflected and transmitted light are at $\sim 7\lambda$ from the metal-sample interface.

Feasible Experimental Setup

In this section, we discuss a feasible experimental setup for practically implementing the proposed technique. The experimental setup for the proposed technique will not be much different from that for a conventional Kretschmann configuration-based sensor. In the proposed technique, the objective will be to measure the change in the optical magnetism rather than the change in the reflection profile as is measured in the conventional technique. We present the feasible experimental setup for the proposed technique in Fig. 1. In experiments, a He–Ne laser can be used as the 633-nm-wavelength light source. A neutral-density filter will be used to change and control the intensity of incident light. A polarizing prism cube (PC) will be used to isolate the p -polarized light from the incident unpolarized light. The p -polarized light will be incident on a convex lens so that it converges and focuses on the metal layer of the sensor. The sensor will be placed on a rotation stage so that the incidence angle of light can be changed. A photometer can record the reflected light intensity and a Ferromaster can record the optical magnetism of the sensor structure. Finally, the reflected light intensity or the optical magnetism of the sensor will be analyzed by a digital analyzer or oscilloscope.

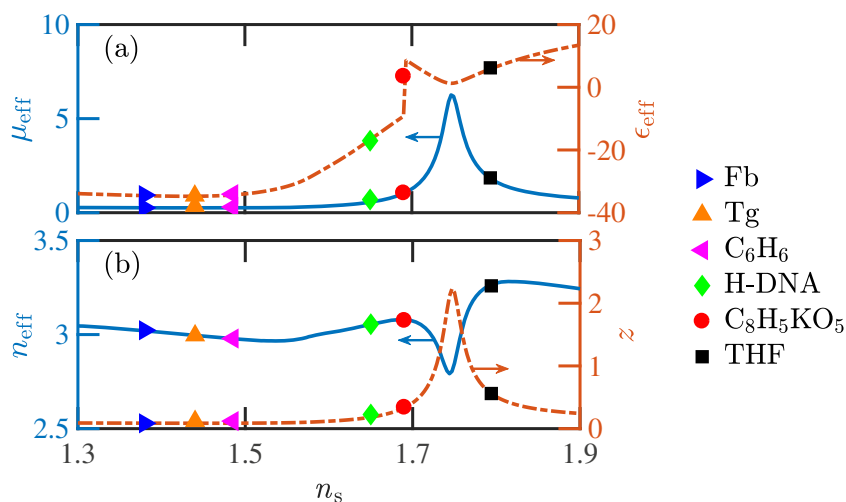
Results and Discussion

Figure 2 illustrates μ_{eff} , ε_{eff} , n_{eff} , and z of the sensor based on Kretschmann configuration that we study in this work as described in the previous section. We vary the refractive index n_s of the sample layer from 1.3 to 1.9. In Fig. 2a, we find that $\mu_{\text{eff}} < 1$ and $\varepsilon_{\text{eff}} < 0$ when $n_s \lesssim 1.69$. Therefore, the sensor structure is non-magnetic when $n_s \lesssim 1.69$. We note that the response of the structure is non-magnetic, i.e., $\mu_{\text{eff}} \leq 1$, when $z \cdot n_{\text{eff}} < 1$, as shown in Fig. 2b [39]. However, the sensor structure becomes magnetic, i.e., $\mu_{\text{eff}} > 1$, when $n_s > 1.69$. The sensor structure shows a magnetic resonance and μ_{eff} reaches maximum at $n_s \approx 1.75$. At magnetic resonance, n_{eff} is minimum and $z \cdot n_{\text{eff}} > 1$, as shown in Fig. 2b, and therefore, the magnetic field becomes strong to create optical magnetism. Also, we note that the magnetic response of the structure is Lorentzian, which verifies the optical magnetism as has also been observed before for planar multi-layer structures [40, 41].

While we investigate the effects of sample layer refractive index on the sensor constitutive parameters in Fig. 2, we present the dynamics of the incident light with the sensor structure in Fig. 3. The results presented in Fig. 3 help to understand the physics of the proposed technique. Figure 3a and b show magnetic field profiles in the vertical cross-section, i.e., in the direction perpendicular to the layer interfaces, of the sensor when $n_s = 1.3$ and $n_s = 1.546$, respectively. We find that dual mode SPPs are excited at the metal-dielectric interface due to the interaction of the incident light with the sensor structure when the structure is non-magnetic. When $n_s \approx n_{\text{prism}}$, strong SPPs are excited. However, we find that the response of the conventional multi-layer planar structure based on Kretschmann configuration is non-magnetic when $n_s \lesssim 1.69$, due to the excitation of dual mode SPPs. By contrast, single mode SPPs are excited when $n_s > 1.69$, and as a result, the structure becomes magnetic. In Fig. 3c, we note the excitation of single mode SPPs when $n_s = 1.75$. The excited single mode SPPs at $n_s = 1.75$ are similar to LSPs, and hence, confine the electromagnetic fields more strongly at the metal-sample layer interface. When $n_s = 1.75$, n_{eff} is minimum due to the maximum power confinement in the metal film. When n_s varies from 1.75 to 1.82, strong LSPs are excited as shown in Fig. 3d. For sensing purpose, both SPPs and LSPs are similar from the detection point-of-view. However, the excitation of LSPs support stronger light confinement, and as a result, can enhance the sensor performance, especially, the FoM [42].

The excited LSPs at the metal-prism and metal-sample layer interfaces of the sensor structure interact with each other through the fields that penetrate into the metal. Magnetic dipoles are created due to anti-phase electric dipole oscillations at the top and bottom of the metal layer.

Fig. 2 Effective constitutive parameters **a** μ_{eff} and ϵ_{eff} , and **b** n_{eff} and z for the Kretschmann-based SPR sensor at 633 nm incident wavelength with n_s varying from 1.3 to 1.9



Although the anti-symmetric resonance is also observed when $n_s > 1.80$, the magnetic resonance weakens and μ_{eff} decreases due to interactions among magnetic dipoles, and therefore, due to the phase retardation of the scattered field with respect to the incident field.

Now, in Fig. 4, we present the changes in μ_{eff} and R when the incidence angles vary. The change in μ_{eff} and R with the incidence angle is crucial in the determination of sensing for such a sensor. In Fig. 4a, we show μ_{eff} as a function of the incidence angle (θ_μ) when $n_s = 1.70$ and 1.71. We note that μ_{eff} has a resonance at $\theta_\mu = 56.56^\circ$ and reaches a maximum value of ~ 6.63 when $n_s = 1.70$, whereas μ_{eff} has a resonance at $\theta_\mu = 56.86^\circ$ and reaches a maximum value of ~ 7.29 when $n_s = 1.71$. Figure 4b shows R profiles against incidence angles (θ_R) of the excitation light when $n_s = 1.70$ and 1.71. The R profiles are commonly used in conventional sensors for the calculation of S and FoM. We note that the resonance angles are slightly different for μ_{eff} and R in Fig. 4a and b. This is because when the resonance occurs, the phase between the incident and reflected light alters. S -parameters retrieval

method computes μ_{eff} at resonance that depends not only on the multi-layer thicknesses but also on the distance between the source and the metal-sample layer interface, and also on the distance between the metal-sample layer interface and the reflection and transmission profile detection planes. By contrast, the calculation of R profile depends only on the multi-layer thickness.

The detection accuracy of a SPR sensor is influenced by the FWHM of μ_{eff} or R profiles. A narrow FWHM of the angle-resolved μ_{eff} and R profiles indicates a high signal-to-noise ratio and precision in the measurement of resonance angles [43]. The FWHM of μ_{eff} profiles shown in Fig. 4a are 1.17° and 1.18° when $n_s = 1.70$ and 1.71, respectively. On the contrary, the FWHM of R profiles shown in Fig. 4b are 2.42° and 2.52° when $n_s = 1.70$ and 1.71, respectively. The increase of FWHM for R from that for μ_{eff} is attributed to the faster damping of SPPs than LSPs. The FWHM values of μ_{eff} and R profiles are plotted in Fig. 5 when n_s varies from 1.70 to 1.82. We note that the FWHM for R is more than a factor of two greater than that for μ_{eff} . This is because the confinement of light at SPR is comparatively lower

Fig. 3 Magnetic field profiles polarized in the z -direction for 633 nm incident wavelength when **a** $n_s = 1.30$, **b** $n_s = 1.546$, **c** $n_s = 1.75$ and **d** $n_s = 1.82$

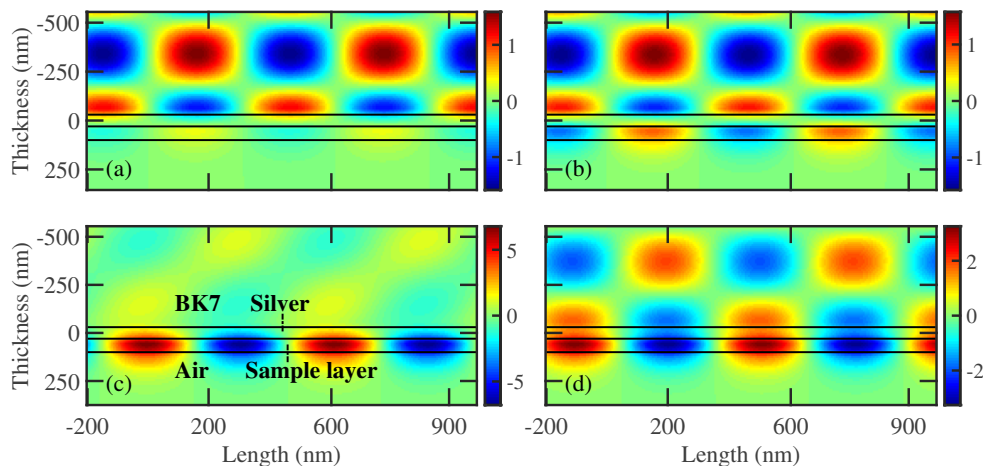
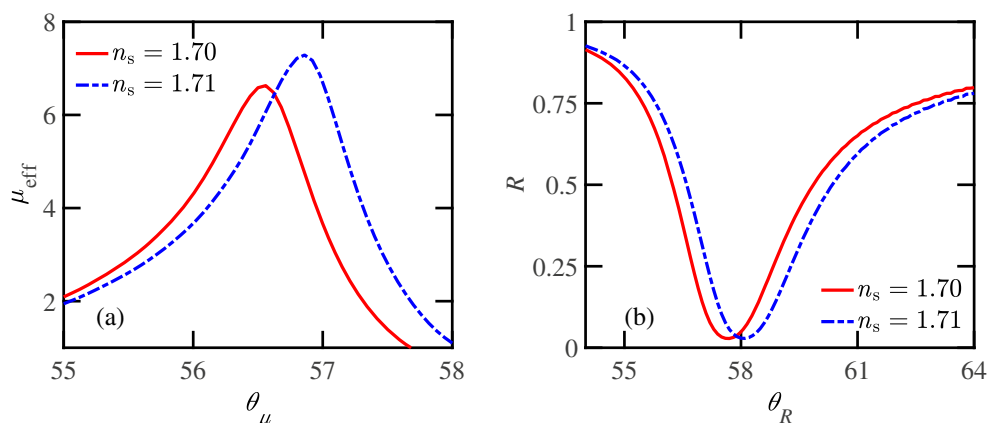


Fig. 4 **a** μ_{eff} and **b** R as functions of resonant incident angles for $n_s = 1.70$ and 1.71 at 633 nm incident wavelength



than that at the magnetic resonance. A better confinement supports lower FWHM value. As n_s increases, FWHM for μ_{eff} decreases while that for R increases.

In Fig. 6a, we show the calculated S from both μ_{eff} and R profiles. The calculated S from μ_{eff} profile is smaller than that from R profile. This is due to low angle shifting property of magnetic resonance. The maximum S calculated using μ_{eff} is $30^\circ/\text{RIU}$ when $n_s = 1.75$. When $n_s > 1.75$, S gradually decreases due to the excitation of anti-symmetric LSP modes. As a result, angle shifting property is reduced. On the other hand, the calculated S from R profile is $47^\circ/\text{RIU}$ when $n_s = 1.75$ and $54^\circ/\text{RIU}$ at the peak when $n_s = 1.78$.

The change in FoM due to the variation of n_s is shown in Fig. 6b. Since the accuracy of detection of a sensor depends on FWHM of the response profile, the most applicable parameter to judge the performance of this kind of devices is FoM. FoM is the mostly used measure for the performance of SPR-based sensors [44–46]. When n_s varies from 1.70 to 1.75 , FoM does not vary much and remains $\sim 24.5 \text{ RIU}^{-1}$ when calculated using μ_{eff} profile. Both S and FoM are maximum when $n_s = 1.75$. When $n_s > 1.75$, FWHM of

μ_{eff} increases, and therefore, FoM decreases. Conversely, FoM $\approx 16 \text{ RIU}^{-1}$ at $n_s = 1.75$, when calculated using R profile. However, the maximum FoM of 17.5 RIU^{-1} is observed at $n_s > 1.75$, when calculated using R profile.

In Table 1, we present a comparison of the FoM obtained from our proposed technique with that of several recently reported sensors that are based on SPR. The FoM of our proposed technique is significantly greater than that of the techniques in Table 1. Moreover, most of the recently reported SPR sensors are based on complex hetero-structures with novel two-dimensional materials. As a result, the fabrication complexity and the cost of these sensors significantly increase, and the performance of these sensors often suffers too. For example, the MoS_2 material included in Ref. [47] incurs energy loss, and hence, a reduced S . Similarly, Refs. [11, 16, 49, 51] include significant complexity without much enhancement in the sensor performance compared to the enhancement obtained by our proposed technique using a simple Kretschmann configuration.

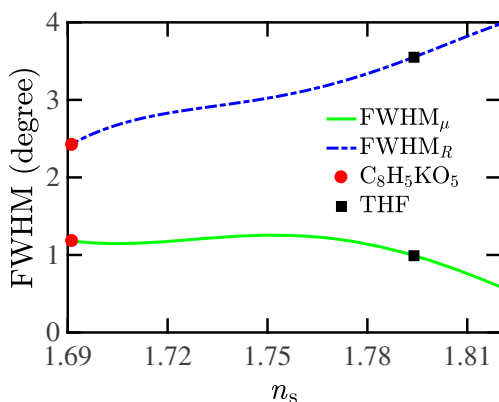


Fig. 5 Variation of FWHM for μ_{eff} and R profiles against n_s . The subscripts μ and R are used when the parameters are calculated using μ_{eff} and R profiles, respectively

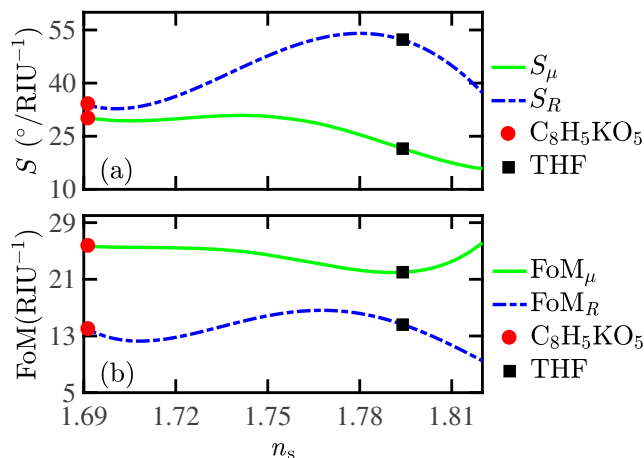


Fig. 6 Variation of **a** S and **b** FoM against n_s . The subscripts μ and R are used when the parameters are calculated using μ_{eff} and R profiles, respectively

Table 1 Comparison of FoM with previously reported sensors

Wavelength (nm)	Enhancement strategy	FoM (RIU ⁻¹)	Reference
633	MoS ₂ nano-sheet	3.44	[47]
633	Graphene-coated Ag with Cr substrate	9.691	[48]
633	Prism-air-MoS ₂ -nano-composite-MoS ₂ -graphene	11.15	[11]
633	Au-graphene-MoS ₂ hybrid	13.13	[49]
630	Au-graphene	14.16	[50]
632.8	SF10-ZiO-Au-MoS ₂ -graphene	15.11	[16]
653.2	SF11L-Au-KCL	16.5	[51]
633	This work (using R)	16	
633	This work (using μ_{eff})	24.50	

It is important to note that the prospect of achieving optical magnetism at visible wavelength by IMI planar structures has recently been a subject of significant interest. In this work, we have determined magnetic resonance of a Kretschmann configuration SPR-based sensor at a specific n_s of the target sample. This magnetic resonance can be created at a lower n_s than that demonstrated in this work, if required, using different 2-D materials such as graphene and MoS₂ on metal surface. We can create magnetic resonance at a different n_s also by nano-structuring of metal and dielectric layers, and optimization of thickness and refractive index of the metal and dielectric layers. Additionally, we can shift the magnetic resonance at a lower n_s also by using a smaller wavelength for the incident light.

Conclusion

We show that strong magnetic resonance can be created in SPR sensors based on Kretschmann configuration. The magnetic response μ_{eff} of the structure can be approximately an order of magnitude greater at resonance than that when out of resonance, which shows promises of the magnetic property of these structures in sensing applications. Thus, using μ_{eff} profiles for sensing could lead to a novel approach for detection of different critical organic and inorganic samples. Our calculations based on S-parameters retrieval method show that the sensor FoM can be greatly increased using the optical magnetism compared to that obtained using the conventional technique in state-of-the-art sensors, which often employ much more complex structures. We believe that the increased sensor performance using optical magnetism resonance in the presence of a target sample from a very simple planar layered structure can lead this approach to applications of sensing of variety of organic and inorganic materials.

References

- Burresi M, Van Oosten D, Kampfrath T, Schoenmaker H, Heideman R, Leinse A, Kuipers L (2009) Probing the magnetic field of light at optical frequencies. *Science* 326(5952):550–553
- Klein MW, Enkrich C, Wegener M, Linden S (2006) Second-harmonic generation from magnetic metamaterials. *Science* 313(5786):502–504
- Shadrivov IV, Kozyrev AB, van der Weide D, Kivshar Y (2008) Nonlinear magnetic metamaterials. *Opt Express* 16(25):20266–20271
- Landau LD, Bell J, Kearsley M, Pitaevskii L, Lifshitz E, Sykes J (2013) *Electrodynamics of continuous media*, vol 8. Elsevier, Amsterdam
- Poddubny A, Iorsh I, Belov P, Kivshar Y (2013) Hyperbolic metamaterials. *Nat Photonics* 7(12):948
- Drachev VP, Podolskiy VA, Kildishev AV (2013) Hyperbolic metamaterials: new physics behind a classical problem. *Opt Express* 21(12):15048–15064
- Krishnamoorthy HN, Jacob Z, Narimanov E, Kretzschmar I, Menon VM (2012) Topological transitions in metamaterials. *Science* 336(6078):205–209
- Papadakis GT, Fleischman D, Davoyan A, Yeh P, Atwater HA (2018) Optical magnetism in planar metamaterial heterostructures. *Nat Commun* 9(1):296
- Chen J, Fan W, Zhang T, Tang C, Chen X, Wu J, Li D, Yu Y (2017) Engineering the magnetic plasmon resonances of metamaterials for high-quality sensing. *Opt Express* 25(4):3675–3681
- Tabasi O, Falamaki C (2018) Recent advancements in the methodologies applied for the sensitivity enhancement of surface plasmon resonance sensors. *Anal Methods* 10(32):3906–3925
- Vahed H, Nadri C (2019) Sensitivity enhancement of spr optical biosensor based on graphene–mos2 structure with nanocomposite layer. *Opt Mater* 88:161–166
- Meng Q-Q, Zhao X, Lin C-Y, Chen S-J, Ding Y-C, Chen Z-Y (2017) Figure of merit enhancement of a surface plasmon resonance sensor using a low-refractive-index porous silica film. *Sensors* 17(8):1846
- Yu Q, Chen S, Taylor AD, Homola J, Hock B, Jiang S (2005) Detection of low-molecular-weight domoic acid using surface plasmon resonance sensor. *Sens Actuators B Chem* 107(1):193–201
- Shalabney A, Abdulhalim I (2012) Figure-of-merit enhancement of surface plasmon resonance sensors in the spectral interrogation. *Opt Lett* 37(7):1175–1177

15. Lopez-Sanchez O, Lembke D, Kayci M, Radenovic A, Kis A (2013) Ultrasensitive photodetectors based on monolayer mos 2. *Nat Nanotechnol* 8(7):497
16. Kushwaha AS, Kumar A, Kumar R, Srivastava S (2018) A study of surface plasmon resonance (spr) based biosensor with improved sensitivity. *PhotNano Fund Appl* 31:99–106
17. Wu L, Guo J, Wang Q, Lu S, Dai X, Xiang Y, Fan D (2017) Sensitivity enhancement by using few-layer black phosphorus-graphene/tmdcs heterostructure in surface plasmon resonance biochemical sensor. *Sens Actuators B Chem* 249:542–548
18. Pal S, Prajapati Y, Saini J, Singh V (2016) Sensitivity enhancement of metamaterial-based surface plasmon resonance biosensor for near infrared. *Optica Applicata* 1:46
19. Maurya J, Prajapati Y, Singh V, Saini J, Tripathi R (2015) Performance of graphene–mos 2 based surface plasmon resonance sensor using silicon layer. *Opt Quant Electron* 47(11):3599–3611
20. Meshginqalam B, Barvestani J (2018) Aluminum and phosphorene based ultrasensitive spr biosensor. *Opt Mater* 86:119–125
21. Sun P, Wang M, Liu L, Jiao L, Du W, Xia F, Liu M, Kong W, Dong L, Yun M (2019) Sensitivity enhancement of surface plasmon resonance biosensor based on graphene and barium titanate layers. *Appl Surf Sci* 475:342–347
22. Caballero B, García-Martín A, Cuevas JC (2016) Hybrid magnetoplasmonic crystals boost the performance of nanohole arrays as plasmonic sensors. *ACS Photonics* 3(2):203–208
23. Zhu Y, Zhang H, Li D, Zhang Z, Zhang S, Yi J, Wang W (2018) Magnetic plasmons in a simple metallic nanogroove array for refractive index sensing. *Opt Express* 26(7):9148–9154
24. Papaioannou ET, Fang H, Caballero B, Akinoglu EM, Giersig M, García-Martín A, Fumagalli P (2017) Role of interactions in the magneto-plasmonic response at the geometrical threshold of surface continuity. *Opt Express* 25(26):32792–32799
25. Simovski CR, Belov PA, He S (2003) Backward wave region and negative material parameters of a structure formed by lattices of wires and split-ring resonators. *IEEE Trans Antennas Propag* 51(10):2582–2591
26. Smith D, Vier D, Koschny T, Soukoulis C (2005) Electromagnetic parameter retrieval from inhomogeneous metamaterials. *Phys Rev E* 71(3):036617
27. Markoš P, Soukoulis C (2003) Transmission properties and effective electromagnetic parameters of double negative metamaterials. *Opt Express* 11(7):649–661
28. Arslanagić S, Hansen TW, Mortensen NA, Gregersen AH, Sigmund O, Ziolkowski RW, Breinbjerg O (2013) A review of the scattering-parameter extraction method with clarification of ambiguity issues in relation to metamaterial homogenization. *IEEE Antennas Propag Mag* 55(2):91–106
29. Chen X, Grzegorzczak TM, Wu B-I, Pacheco Jr, Kong JA (2004) Robust method to retrieve the constitutive effective parameters of metamaterials. *Phys Rev E* 70(1):016608
30. Mayer S (2019) Magnetic permeability meter ferromaster. (accessed January 20, 2020). [Online]. Available: <https://stefan-mayer.com/en/products/permeability-meters.html>
31. Zhao X, Huang T, Ping P, Wu X, Huang P, Pan J, Wu Y, Cheng Z (2018) Sensitivity enhancement in surface plasmon resonance biochemical sensor based on transition metal dichalcogenides/graphene heterostructure. *Sensors* 18(7):2056
32. Mukhtar W, Menon PS, Shaari S, Malek M, Abdullah A (2013) Angle shifting in surface plasmon resonance: experimental and theoretical verification. In: *Journal of physics: conference series*, vol 431. IOP Publishing, p 012028
33. Zeng S, Hu S, Xia J, Anderson T, Dinh X-Q, Meng X-M, Coquet P, Yong K-T (2015) Graphene–mos2 hybrid nanostructures enhanced surface plasmon resonance biosensors. *Sens Actuators B Chem* 207:801–810
34. Xu H, Wu L, Dai X, Gao Y, Xiang Y (2016) An ultra-high sensitivity surface plasmon resonance sensor based on graphene-aluminum-graphene sandwich-like structure. *J Appl Phys* 120(5):053101
35. Omair Z, Talukder MA (2019) Sensitivity analysis of gold nanorod biosensors for single molecule detection. *Plasmonics* 14(6):1611–1619
36. Das A, Talukder MA (2018) Theoretical analysis of bimetallic nanorod dimer biosensors for label-free molecule detection. *AIP Adv* 8(2):025302
37. Jiang H, Choudhury S, Kudyshev ZA, Wang D, Prokopenko LJ, Xiao P, Jiang Y, Kildishev AV (2019) Enhancing sensitivity to ambient refractive index with tunable few-layer graphene/hbn nanoribbons. *Photonics Res* 7(7):815–822
38. Rodrigo D, Limaj O, Janner D, Etezadi D, De Abajo FJG, Pruneri V, Altug H (2015) Mid-infrared plasmonic biosensing with graphene. *Science* 349(6244):165–168
39. Smith DR, Schultz S, Markoš P, Soukoulis C (2002) Determination of effective permittivity and permeability of metamaterials from reflection and transmission coefficients, vol 65
40. Rockstuhl C, Lederer F, Etrich C, Pertsch T, Scharf T (2007) Design of an artificial three-dimensional composite metamaterial with magnetic resonances in the visible range of the electromagnetic spectrum, vol 99
41. Petrakis L (1967) Spectral line shapes: Gaussian and lorentzian functions in magnetic resonance. *J Chem Educ* 44(8):432
42. Ho Y-L, Lee Y, Maeda E, Delaunay J-J (2013) Coupling of localized surface plasmons to u-shaped cavities for high-sensitivity and miniaturized detectors. *Opt Express* 21(2):1531–1540
43. Chen Z, Zhao X, Lin C, Chen S, Yin L, Ding Y (2016) Figure of merit enhancement of surface plasmon resonance sensors using absentee layer. *Appl Opt* 55(25):6832–6835
44. Maccaferri N, Gregorczyk KE, De Oliveira TV, Kataja M, Van Dijken S, Pirzadeh Z, Dmitriev A, Åkerman J, Knez M, Vavassori P (2015) Ultrasensitive and label-free molecular-level detection enabled by light phase control in magnetoplasmonic nanoantennas. *Nat Commun* 6:6150
45. Otte MA, Sepulveda B, Ni W, Juste JP, Liz-Marzán LM, Lechuga LM (2009) Identification of the optimal spectral region for plasmonic and nanoplasmonic sensing. *ACS Nano* 4(1):349–357
46. Shen Y, Zhou J, Liu T, Tao Y, Jiang R, Liu M, Xiao G, Zhu J, Zhou Z-K, Wang X et al (2013) Plasmonic gold mushroom arrays with refractive index sensing figures of merit approaching the theoretical limit. *Nat Commun* 4:2381
47. Ouyang Q, Zeng S, Jiang L, Hong L, Xu G, Dinh X-Q, Qian J, He S, Qu J, Coquet P et al (2016) Sensitivity enhancement of transition metal dichalcogenides/silicon nanostructure-based surface plasmon resonance biosensor. *Sci Rep* 6:28190
48. Verma A, Prakash A, Tripathi R (2015) Sensitivity enhancement of surface plasmon resonance biosensor using graphene and air gap. *Opt Commun* 357:106–112
49. Rahman MS, Anower MS, Hasan MR, Hossain MB, Haque MI (2017) Design and numerical analysis of highly sensitive au-mos2-graphene based hybrid surface plasmon resonance biosensor. *Opt Commun* 396:36–43
50. Chen S, Lin C (2019) Figure of merit analysis of graphene based surface plasmon resonance biosensor for visible and near infrared. *Opt Commun* 435:102–107
51. Chen J, Tang C, Mao P, Peng C, Gao D, Yu Y, Wang Q, Zhang L (2016) Surface-plasmon-polaritons-assisted enhanced magnetic response at optical frequencies in metamaterials. *IEEE Photonics J* 8(1):1–7

Publisher's Note Springer Nature remains neutral with regard to jurisdictional claims in published maps and institutional affiliations.